Tight-binding model for GaAs/AlAs resonant-tunneling diodes

Timothy B. Boykin, Jan P. A. van der Wagt, and James S. Harris, Jr.
Department of Electrical Engineering, Stanford University, Stanford, California 94305
(Received 17 September 1990)

Models of resonant-tunneling diodes based on the envelope-function approximation often give unsatisfactory results. In order to address some of the shortcomings of these models, we employ a tight-binding model that allows more careful treatment of heterointerfaces than is possible in the envelope-function approach. We use transfer matrices to carry out the calculation and present an improved method that allows us to transfer across larger device dimensions (> 1000 Å), thereby permitting us to include space-charge regions in the model. We compare results obtained with the tight-binding and envelope-function approximations.

I. INTRODUCTION

It is widely known that models of resonant-tunneling diodes (RTD's) based on the envelope-function approximation produce values of the valley current which are far smaller than what one measures in a real device. This discrepancy is especially pronounced in devices with AlAs barriers, due to the relatively small conduction-band discontinuity between the GaAs Γ valley the AlAs X valley. In order to model such devices more accurately, one must treat the heterointerfaces more carefully than is possible in the usual envelope-function model, taking into account the fact that the electron has many tunneling paths available to it. To address this shortcoming, one might try to extend the envelope-function approximation to include valley-mixing effects at a heterointerface. This has been the approach of Ando *et al.*[1,2] Another option is to discard the envelope-function approach altogether, restating the problem in terms of localized states, for example. In this work, we employ an empirical tight-binding model to treat heterostructures lacking translational symmetry in one direction.

Tight-binding models have been used to study single interfaces[3] and superlattices[4] and, less frequently, RTD's (Ref. 5) and quantum wells. Because all these structures involve a lack of translational invariance on an atomic scale, a transfer-matrix[6,7] approach is commonly used. It is well known that transfer matrices, such as those used in these types of calculations, are fraught with numerical instabilities, namely, exponential blowup. Schulman and Chang[8] have addressed this problem for superlattices and bound states of quantum wells with their reduced-Hamiltonian method; it has, however, remained a serious obstacle for aperiodic structures with unbound states, such as RTD's. As a result, the few published RTD models can handle only relatively small dimensions (Ref. 5 uses 60 monolayers, or 170 Å), and thus cannot incorporate any of the space-charge regions which form on either side of the RTD. Since the accumulation layer in front of a RTD can cause band bending of about 0.1 eV under moderate bias, it is essential that these effects be included in the model. We have recently discovered a method for solving transfer-matrix problems which can handle relatively long lengths of material; we regularly model structures of about 300 monolayers (849 Å) and have done calculations for devices as large as 400 monolayers (1132 Å). The only limitations we have found are computer time and money.

In this work, we examine RTD's using a nearest-neighbor-only tight-binding model, including depletion and accumulation regions, and compare our results to those obtained with the usual envelope-function approximation. In addition, we briefly discuss some of the difficulties and virtues of such an approach. We use transfer matrices,[6,7] with the aforementioned improved solution method. In Sec. II, we briefly discuss our transfer matrix, which is somewhat simpler than that of Refs. 6 and 7. In Sec. III, we present our enhancement to the usual transfer-matrix approach and apply it to RTD's and discuss the results.

II. TRANSFER-MATRIX METHOD AND TIGHT-BINDING MODEL

In order to study systems lacking translational symmetry in the z direction, we use the transfer-matrix method.[6,7] We employ a nearest-neighbor-only, empirical tight-binding model with a basis of five atomiclike orbitals per atom, s, p_x, p_y, p_z, and s^*, where the last orbital is an excited s state.[9] Additionally, we specialize to the case of zinc-blende-structure crystals, giving ten orbitals per unit cell, and we consider only materials oriented in the [001] direction. Figure 1 illustrates our definition of a layer. In each layer L we construct Bloch sums of each orbital type centered on both anions and cations which have the requisite symmetry in the x-y plane:

$$|na;\mathbf{k}_{\|};L\rangle=\sum_j \exp[i\mathbf{k}_{\|}\cdot\mathbf{R}_{j\|}]|na;L;\mathbf{R}_{j\|}\rangle\ , \tag{1}$$

$$|nc;\mathbf{k}_{\|};L\rangle=\sum_j \exp[i\mathbf{k}_{\|}\cdot(\mathbf{R}_j+\mathbf{v})_{\|}]|nc;L;(\mathbf{R}_j+\mathbf{v})_{\|}\rangle\ . \tag{2}$$

The index n is one of s, p_x, p_y, p_z, or s^*. The letters "a" and "c" signify anion and cation, respectively. The notation $\mathbf{r}_\parallel$ signifies the projection of $\mathbf{r}$ onto the x-y plane, so that the sums in (1) and (2) are in a plane parallel to the x-y plane. In (2), $\mathbf{v}$ is the basis vector of a unit cell: $\mathbf{v}=a(\mathbf{x}+\mathbf{y}+\mathbf{z})/4$, where a is the lattice constant. We write the total wave function, which is a simultaneous eigenstate of the Hamiltonian $\mathcal{H}$ and $\mathbf{k}_\parallel$ as

$$|\Psi_{\mathbf{k}_\parallel}\rangle=\sum_L\sum_n\left(C_L^{na}|na;\mathbf{k}_\parallel;L\rangle+C_L^{nc}|nc;\mathbf{k}_\parallel;L\rangle\right). \quad (3)$$

We have suppressed the normalization in (1)–(3) because it is not important. The transpose of a vector of coefficients $\mathbf{C}_L$ is defined by

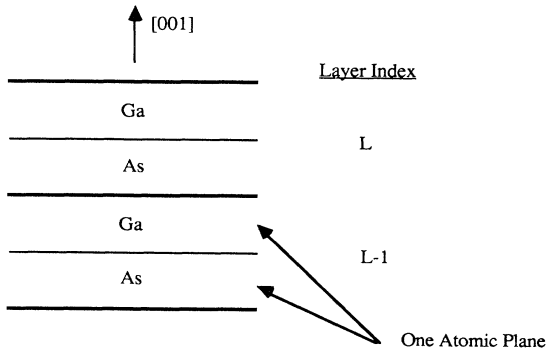

FIG. 1. GaAs oriented in the [001] direction.

$$(\mathbf{C}_L)^T=(C_L^{sa},C_L^{xa},C_L^{ya},C_L^{za},C_L^{s^*a},C_L^{sc},C_L^{xc},C_L^{yc},C_L^{zc},C_L^{s^*c}), \quad (4)$$

where we have used the shorthand "x" for p_x, etc. We then employ the transfer matrix $\underline{\mathcal{T}}$, which is generated by taking inner products of (1) and (2) with the Schrödinger equation $[\mathcal{H}-E]|\Psi_{\mathbf{k}_\parallel}\rangle=0$ to relate the various $\mathbf{C}_L$ to one another. Instead of the general expressions given in Ref. 6, we obtain a simpler relationship, resulting from our inclusion of only nearest-neighbor interactions:

$$\mathbf{C}_L=\underline{\mathcal{T}}\mathbf{C}_{L-1}. \quad (5)$$

It turns out that in the nearest-neighbor approximation, for certain values of $\mathbf{k}_\parallel$, $\underline{\mathcal{T}}$ will not exist. This situation is not due to a defect in the transfer-matrix method, but rather is merely reflective of the pathologies present in the underlying tight-binding Hamiltonian. This is easily demonstrated for the case under consideration by choosing a $\mathbf{k}_\parallel$ for which $\underline{\mathcal{T}}$ does not exist (for the nearest-neighbor-only approximation in a [001]-oriented crystal, $\mathbf{k}_\parallel=(2\pi/a)\mathbf{x}$, for example), and computing the determinant of the matrix $[\underline{\mathcal{H}}-E\underline{1}]$, with $\mathbf{k}=(2\pi/a)\mathbf{x}+k_z\mathbf{z}$. (The Hamiltonian in the nearest-neighbor tight-binding approximation is given in Ref. 9.) We used MAPLE (Ref. 10) to symbolically evaluate the determinant, and found it completely independent of k_z, regardless of the choice of tight-binding parameters, meaning that for this $\mathbf{k}_\parallel$, the electron is both stationary and infinitely massive for motion in the z direction. It is therefore no surprise that $\underline{\mathcal{T}}$ does not exist for certain $\mathbf{k}_\parallel$. In spite of this pathology, the nearest-neighbor approximation is still valuable. It will not be seriously in error when $\mathbf{k}_\parallel$ is small, as is the case at low temperatures, and, due to the N^3 scaling of most matrix operations, it is much more computationally accessible than even a second-near-neighbor model.

Since interfaces and/or applied biases are present in all structures of interest, it is appropriate to briefly discuss our treatment of these features. At an interface, we take the tight-binding parameters to be the average of those in the two bulk materials on either side, ensuring that the product of transfer matrices representing a unit cell of a

TABLE I. Tight-binding parameters. All values are in eV. The parameters are used in the nearest-neighbor tight-binding Hamiltonian given in Ref. 9.

Parameter	GaAs	AlAs
$E(sa)$	−8.390 00	−8.266 311 0
$E(pa)$	1.074 75	0.344 288 7
$E(sc)$	−2.654 05	−1.629 823 0
$E(pc)$	3.554 75	2.947 689 0
$E(s^*a)$	8.574 75	6.844 239 0
$E(s^*c)$	6.704 75	6.087 689 0
$V(s,s)$	−6.451 3	−6.664 2
$V(x,x)$	1.954 6	1.878 0
$V(x,y)$	4.770 0	3.860 0
$V(sa,pc)$	4.680 0	5.600 0
$V(pa,sc)$	7.700 0	7.600 0
$V(s^*a,pc)$	4.850 0	4.220 0
$V(pa,s^*c)$	6.900 0	8.300 0

TABLE II. Energies, minima, and effective masses. Energies are in eV. Wave vectors are in Å^{-1}. Effective masses are expressed in terms of the free-electron rest mass. Refer to Fig. 2 for energy gaps.

Quantity	GaAs	AlAs
E_g	1.538	3.136
$E_{c,\min}(\Gamma)$	1.538	2.497
$E_{X\Gamma}$	0.484	−0.882
E_{XX}	0.268	0.542
$k_{\min}$ in [001]	0.9639	0.8512
m_Γ^*	0.0689	0.1582
$m_{X,l}^*$	1.457	1.046

superlattice $\underline{\mathcal{T}}$ has the necessary similarity property $\underline{\mathcal{T}}^{-1} \sim \underline{\mathcal{T}}^{\dagger}$. We treat an applied bias as a stepwise-constant potential.

Our tight-binding parameters are given in Table I. We arrived at this particular choice of parameters by starting with those given in Refs. 4 and 9, but modifying them to give better longitudinal X-valley effective masses. The AlAs parameters have been adjusted to make the GaAs/AlAs valence-band discontinuity 40% of the energy-gap difference at the Γ point. In Table II, we list the energy gaps and effective masses generated by the tight-binding parameters of Table I. The lowest two of

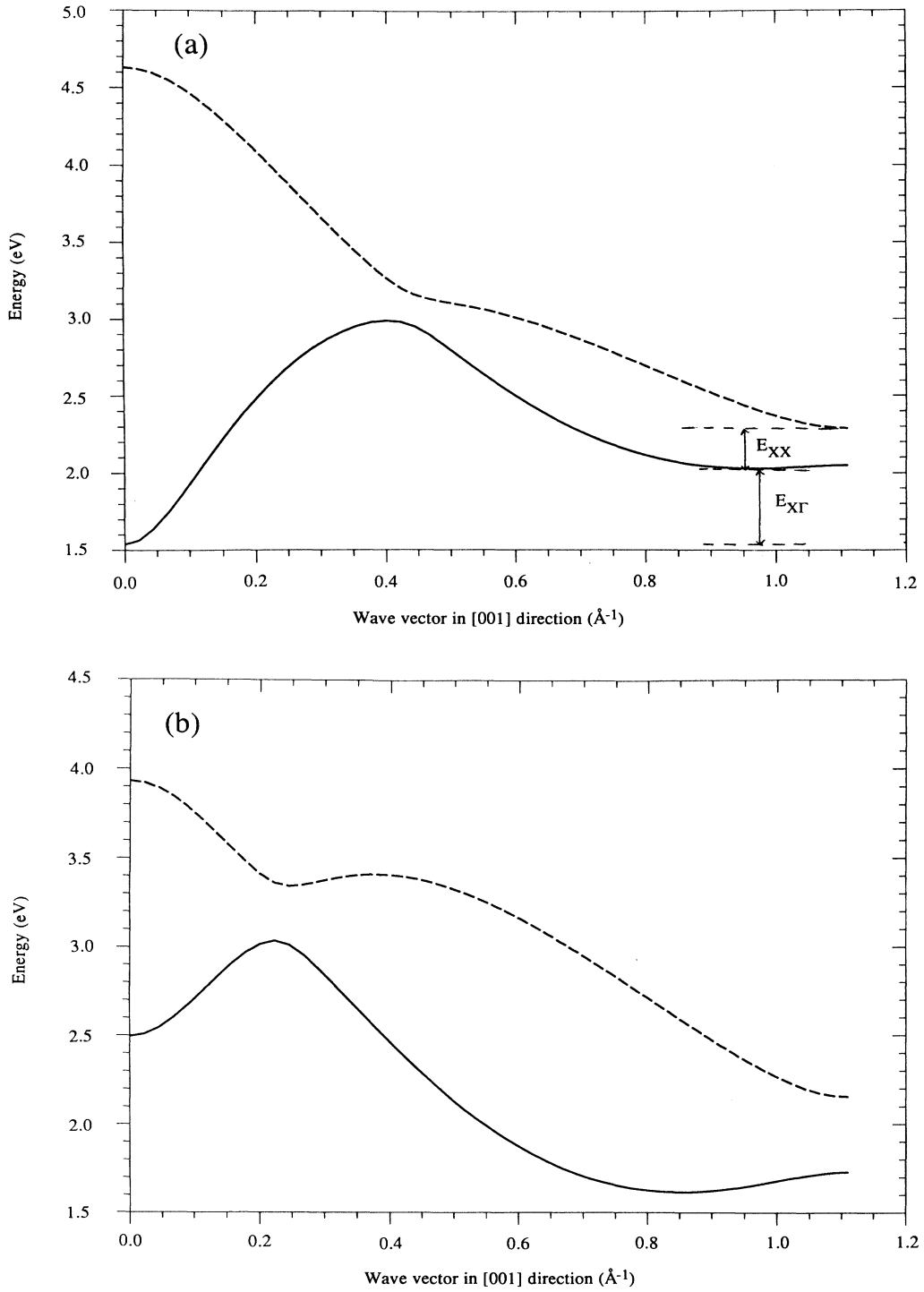

FIG. 2. (a) The two lowest conduction bands of GaAs from Γ to X from our tight-binding parameters. (b) The two lowest conduction bands of AlAs from Γ to X from our tight-binding parameters.

the six conduction bands, along with some of the gaps, are shown in Fig. 2.

III. APPLICATION TO RESONANT-TUNNELING DIODES

A. General

For a RTD, we carry out an expansion in terms of bulk GaAs transfer-matrix eigenstates on either side of the structure in the first layer after the band-bending associated with the space-charge regions has essentially stopped. The left-hand-side expansion states will be those with bulk transfer-matrix eigenvalues λ such that $|\lambda|>1$ (decaying as one transfers with $\underline{\mathcal{T}}^{-1}_{\text{GaAs,left}}$ toward $z\rightarrow-\infty$) and those propagating states with $\partial E/\partial k_z<0$, where $\lambda=\exp(ik_z a/2)$ (reflected states). We label these states $\mathbf{v}_6,\ldots,\mathbf{v}_{10}$. In addition, there will be an incident electron. We assume that it is in a bulk transfer-matrix eigenstate, say $\mathbf{v}_1$, with $\partial E/\partial k_z>0$. We furthermore restrict our attention to cases in which this is the only forward-propagating state on the left-hand side. In these cases, there will be only one reflected state. The right-hand-side expansion states will be those with $|\lambda|<1$ (decaying as one propagates with $\underline{\mathcal{T}}_{\text{GaAs,right}}$ toward $z\rightarrow+\infty$) and those propagating states with $\partial E/\partial k_z>0$ (transmitted states). We label these states $\mathbf{u}_1,\ldots,\mathbf{u}_5$. (Note that it is possible to have several transmitted states.) We must then solve the linear system:

$$\underline{\mathcal{T}}_{\text{tot}}(\mathbf{v}_1+b_6\mathbf{v}_6+\cdots+b_{10}\mathbf{v}_{10})=b_1\mathbf{u}_1+\cdots+b_5\mathbf{u}_5\ , \tag{6}$$

$$(\mathbf{u}_1|\cdots|\mathbf{u}_5|-\underline{\mathcal{T}}_{\text{tot}}\mathbf{v}_6|\cdots|-\underline{\mathcal{T}}_{\text{tot}}\mathbf{v}_{10})\begin{pmatrix}b_1\\ \vdots\\ b_{10}\end{pmatrix}=(\underline{\mathcal{T}}_{\text{tot}}\mathbf{v}_1)\ . \tag{7}$$

Now, since $\langle n|p_z|n\rangle=(m_0/\hbar)\partial E_n/\partial k_{z,n}$,[11] the transmitted probability current J_z is constant and is given by

$$J_z=\frac{1}{\hbar L_z}\sum_n |b_n|^2\frac{\partial E_n}{\partial k_{z,n}}\ , \tag{8}$$

where L_z is a normalization length and the sum is over transmitted states. An analogous expression holds for the reflected current. From (8), we see that the transmission and reflection coefficients for transport from left to right are given by

$$T_{LR}(E,\mathbf{k}_\parallel)=\sum_j |b_j|^2\frac{|\partial E/\partial k_z|_j}{|\partial E/\partial k_z|_{\text{inc}}}\ , \tag{9}$$

$$R_{LR}(E,\mathbf{k}_\parallel)=|b_6|^2\ . \tag{10}$$

Note that the sum in (9) is over forward-propagating output-side expansion states only, and that "inc" denotes the incident state. In (10), note that if there can be only one incident state, there will be one and only one reflected state, and this state will have the same magnitude of group velocity as the incident state. Finally, the sum of (9) and (10) is always unity.

B. Improved method

As mentioned in the Introduction, the straightforward implementation of Eq. (6), Eq. (7), will only work if the composite transfer matrix $\underline{\mathcal{T}}_{\text{tot}}$ is a product of a relatively small number of single-monolayer transfer matrices. We have typically found this number to be 20–30 when using double precision. (It will naturally be much less when $\mathbf{k}_\parallel$ approaches one of the pathologies of the underlying bulk tight-binding Hamiltonian.) Schulman and Chang[8] discuss the reasons for this instability in connection with their reduced-Hamiltonian method, which also employs transfer matrices. Their solution is to periodically reexpand the product of transfer matrices in terms of a new basis, normalized to counteract the exponential growth. Since RTD's necessarily include continuum states, and the reduced-Hamiltonian method cannot be applied to such states,[8] we must seek a different solution to the numerical instability.

We now present our method for dealing with the exponential growth problem. First, rewrite $\underline{\mathcal{T}}_{\text{tot}}$ as a product of composite transfer matrices $\underline{\mathcal{T}}_i$, $i=1,2,\ldots,n$, each of which is itself a product of m_i single-monolayer transfer matrices, where each m_i is less than the total number of monolayers which can be successfully handled by a straightforward implementation such as Eq. (7):

$$\underline{\mathcal{T}}_{\text{tot}}=\underline{\mathcal{T}}_n\underline{\mathcal{T}}_{n-1}\cdots\underline{\mathcal{T}}_2\underline{\mathcal{T}}_1\ . \tag{11}$$

Equation (6) may then be rewritten as

$$\underline{\mathcal{T}}_1(\mathbf{v}_1+b_6\mathbf{v}_6+\cdots+b_{10}\mathbf{v}_{10})=\underline{\mathcal{T}}_2^{-1}\underline{\mathcal{T}}_3^{-1}\cdots\underline{\mathcal{T}}_n^{-1}(b_1\mathbf{u}_1+\cdots+b_5\mathbf{u}_5)\ . \tag{12}$$

Now we expand the right-hand side of (12) in terms of some basis. Any basis will suffice—it need not be specially normalized as is the case with the basis used to extend the reduced-Hamiltonian method.[8] Accordingly, we employ the standard basis $\{\mathbf{e}_i\}$, where the column vector $\mathbf{e}_i$ has a 1 in the ith row and 0 elsewhere. Thus, whereas we previously had 10 equations (12), now we have 20:

$$\underline{\mathcal{T}}_1(\mathbf{v}_1+b_6\mathbf{v}_6+\cdots+b_{10}\mathbf{v}_{10})=c_1^{(2)}\mathbf{e}_1+\cdots+c_{10}^{(2)}\mathbf{e}_{10}\ , \tag{13}$$

$$\underline{\mathcal{T}}_2(c_1^{(2)}\mathbf{e}_1+\cdots+c_{10}^{(2)}\mathbf{e}_{10})=\underline{\mathcal{T}}_3^{-1}\underline{\mathcal{T}}_4^{-1}\cdots\underline{\mathcal{T}}_n^{-1}(b_1\mathbf{u}_1+\cdots+b_5\mathbf{u}_5)\ , \tag{14}$$

where the $c_j^{(i)}$ are new expansion coefficients. If we repeat the above process until $\underline{\mathcal{T}}_n$ appears on the left-hand side, we obtain $10n$ equations, arranged in matrix form:

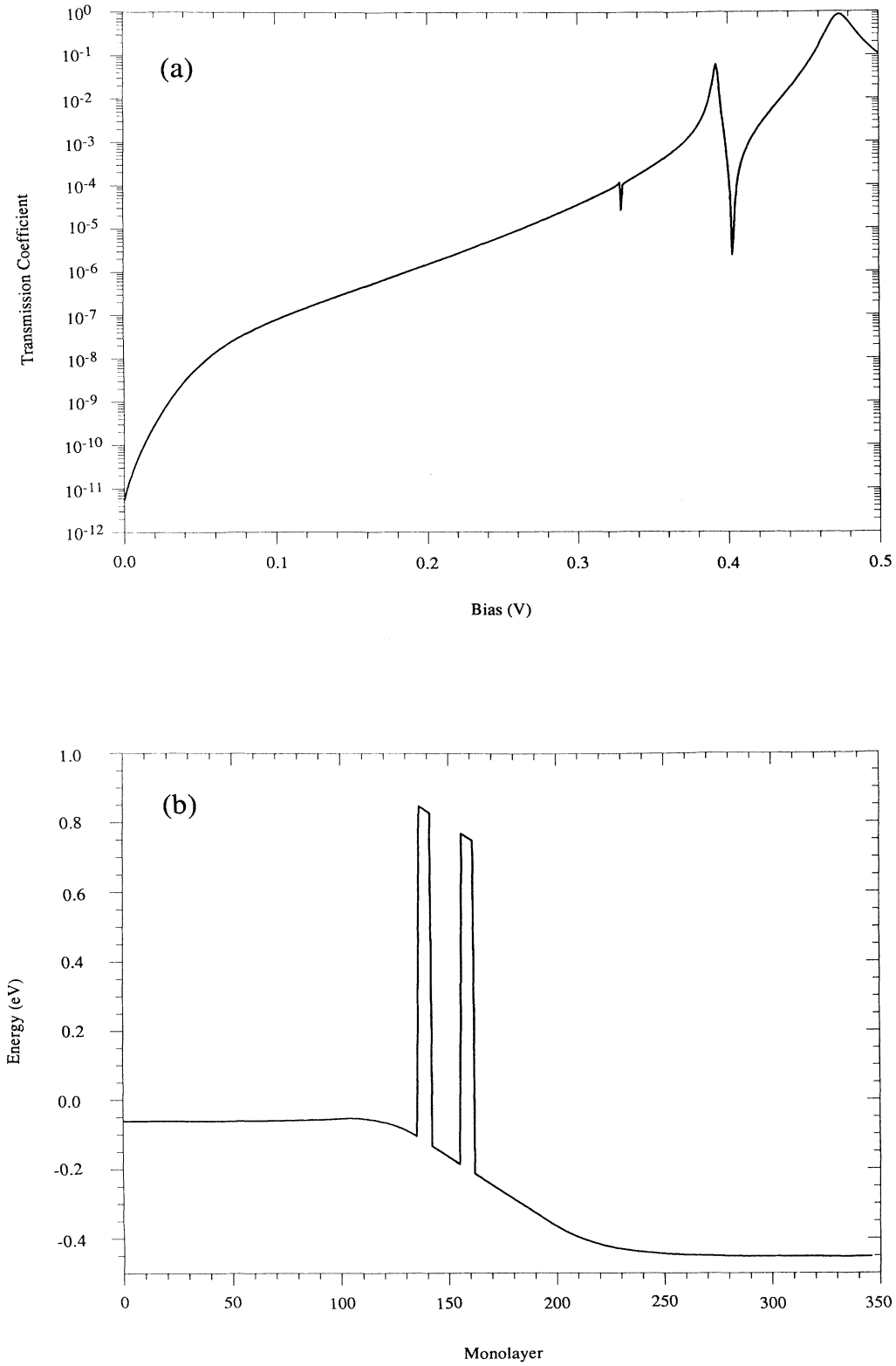

FIG. 3. (a) Transmission coefficient of a double-barrier RTD with 6-monolayer AlAs barriers, a 14-monolayer GaAs well, and 35-monolayer undoped emitter and collector spacers. We assume $T=77$ K, $N_D=10^{18}$ cm^{-3}, and complete donor ionization. The electron is incident from the Γ valley of the GaAs emitter with $\mathbf{k}_{\parallel}=\mathbf{0}$ and $E=5.5058$ meV above the conduction-band minimum. (b) Potential profile used in solving the Schrödinger equation for the same RTD at 0.392 V bias.

$$\begin{bmatrix} \underline{\mathcal{A}}_{1,1} & \underline{1} & \underline{0} & \cdots & \cdots & \underline{0} \\ \underline{0} & -\underline{\mathcal{T}}_2 & \underline{1} & \ddots & \ddots & \vdots \\ \vdots & \underline{0} & -\underline{\mathcal{T}}_3 & \ddots & \ddots & \vdots \\ \vdots & \ddots & \ddots & \ddots & \ddots & \underline{0} \\ \underline{0} & \ddots & \ddots & \ddots & \ddots & \underline{1} \\ \underline{\mathcal{A}}_{n,1} & \underline{0} & \cdots & \cdots & \underline{0} & -\underline{\mathcal{T}}_n \end{bmatrix} \begin{bmatrix} \mathbf{b} \\ \mathbf{c}^{(2)} \\ \vdots \\ \mathbf{c}^{(n)} \end{bmatrix} = \begin{bmatrix} \underline{\mathcal{T}}_1 \mathbf{v}_1 \\ \mathbf{0} \\ \vdots \\ \mathbf{0} \end{bmatrix}, \quad (15)$$

where each $\underline{1}$ is a 10×10 identity matrix, each block above is 10×10, $\mathbf{b}$ and the $\mathbf{c}^{(i)}$ are given by

$$\mathbf{b}=\begin{bmatrix} b_1 \\ \vdots \\ b_{10} \end{bmatrix}, \quad \mathbf{c}^{(i)}=\begin{bmatrix} c_1^{(i)} \\ \vdots \\ c_{10}^{(i)} \end{bmatrix}, \quad (16)$$

and the $\underline{\mathcal{A}}$'s are

$$\underline{\mathcal{A}}_{1,1}=(\mathbf{0}|\mathbf{0}|\mathbf{0}|\mathbf{0}|\mathbf{0}|-\underline{\mathcal{T}}_1\mathbf{v}_6|\cdots|-\underline{\mathcal{T}}_1\mathbf{v}_{10}), \quad (17)$$

$$\underline{\mathcal{A}}_{n,1}=(\mathbf{u}_1|\cdots|\mathbf{u}_5|\mathbf{0}|\mathbf{0}|\mathbf{0}|\mathbf{0}|\mathbf{0}). \quad (18)$$

Note that we must not solve (15) by block-elimination methods, for those methods will put the instabilities right back into the problem. [This may be seen by attempting block Gaussian elimination on (15).] On the other hand, any other sparse Gaussian elimination algorithm[12] should solve (15) without reintroducing the instabilities, thus allowing us to use transfer matrices over sufficient distances (approximately 1000 Å) to include space-charge regions. The reason why the rearrangement, Eq. (15), works so well is simply that by limiting the number of single-monolayer transfer-matrix factors in each composite transfer matrix $\underline{\mathcal{T}}_i$ we have effectively reduced the exponential growth to a tolerable level.

C. Results and discussion

Figure 3(a) is a graph of the transmission coefficient as calculated from (9) versus applied bias for a RTD with 6-monolayer AlAs barriers and a 14-monolayer GaAs well. The device also has 35-monolayer undoped emitter and collector spacers, and the emitter and collector are both doped to $N_D=10^{18}$ cm^{-3}. The total amount of material included in the calculation was 346 monolayers (979 Å). We take $T=77$ K and assume complete donor ionization, due to the heavy doping. The potential profile for the Schrödinger equation is calculated with the Poisson equation. The charge term arises from the ionized donors and the electrons, which obey Fermi-Dirac statis-

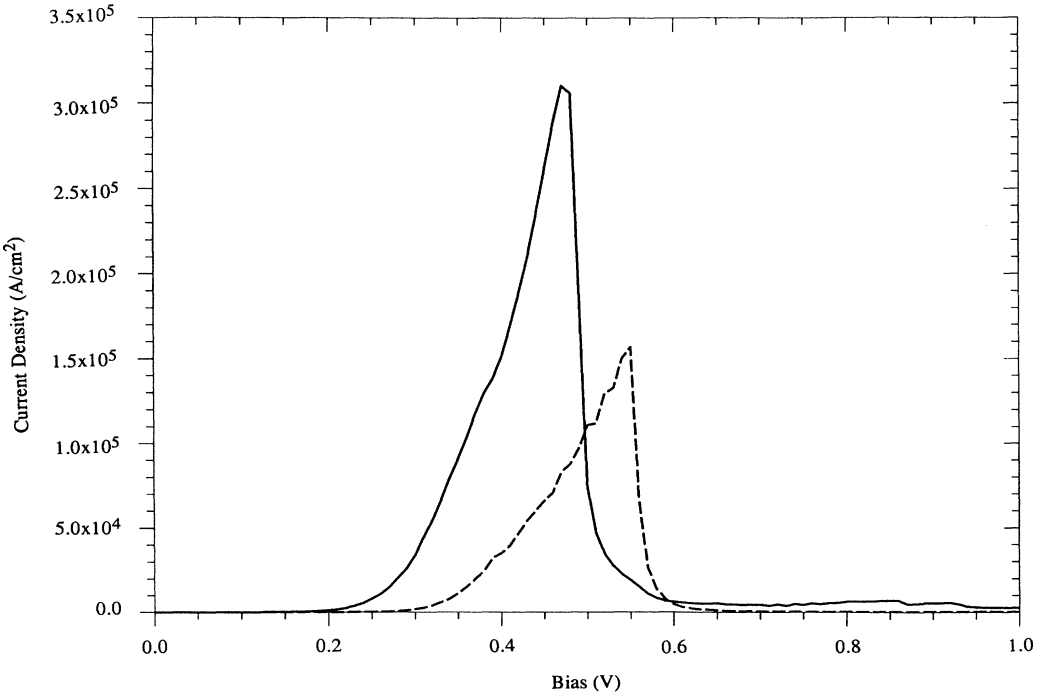

FIG. 4. Current density vs voltage graph for the device of Fig. 3. Solid line, tight-binding calculation; dashed line, envelope-function calculation.

tics. That is, the Poisson and Schrödinger equations were not solved self-consistently. Figure 3(b) shows the potential profile used for $V=0.392$ V. The electron is incident from the Γ valley of the GaAs emitter with $\mathbf{k}_{\parallel}=\mathbf{0}$ and $E-E_c=5.5058$ meV ($k_z=0.01$ Å^{-1}). For all points in the graph, flux conservation was excellent, giving $R+T=1.0\pm10^{-5}$. The graph shows an interesting structure, particularly the resonance and antiresonance at 0.392 and 0.403 V, respectively. This type of structure, which is not observed in the usual envelope-function calculations (but which is found in calculations based on the method of Ando *et al.*[1,2]) is associated with tunneling through virtual states in the X valley of the second barrier. This is demonstrated by expanding the wave function in one layer of the second barrier in terms of the eigenstates of the bulk AlAs transfer matrix for that layer and examining the resulting expansion coefficients. For the aforementioned RTD we carried out such an expansion in the last layer of the second barrier at the resonant bias of 0.392 V and found that the major contributions (totaling over 95%) come from X-valley Bloch (propagating) states with $k_z=\pm0.710$ and ±1.02 Å^{-1}.

We have also calculated the tunneling current for this device. The transmission coefficient in the tight-binding model is a function of E, $\mathbf{k}_{\parallel}$, and applied bias V. Thus the current is given by the triple integral

$$J=\frac{2e}{(2\pi)^3\hbar}\int_{\mathrm{BZ}}\int\left[\int_{E_{c,\min}(\mathbf{k}_{\parallel})}^{E_{c,\max}(\mathbf{k}_{\parallel})}[f_E(E)-f_C(E)]\times T(E,\mathbf{k}_{\parallel},V)dE\right]dk_y dk_x\ , \tag{19}$$

where f_E and f_C are Fermi-Dirac distribution functions for the emitter and collector bulklike regions, respectively. While Eq. (19) gives the proper expression for the current, it is exceedingly difficult to evaluate numerically, owing to the great amount of work necessary to calculate the transmission coefficients. We reduce (19) to a single integral by making the approximation

$$T(E,\mathbf{k}_{\parallel},V)\rightarrow T(E-E_{\parallel},\mathbf{0},V)\ , \tag{20}$$

where $E_{\parallel}=\hbar^2\mathbf{k}_{\parallel}^2/2m^*_{\mathrm{GaAs}}$. We may then use the standard expression[13] for the tunneling current

$$J=\frac{em^*_{\mathrm{GaAs}}k_BT}{2\pi^2\hbar^3}\times\int_0^{\infty}T(E_1,V)\times\ln\left[\frac{1+\exp[(E_{F,E}-E_1)/k_BT]}{1+\exp[(E_{F,E}-E_1-\mathrm{eV})/k_BT]}\right]dE_1\ , \tag{21}$$

where $E_{F,E}$ is the Fermi level in the emitter bulklike region.

Figure 4 is a graph of the current density versus applied bias for the structure of Fig. 3, calculated with both the tight-binding (solid line) and envelope-function (dashed line) models. The envelope-function calculation made no corrections for conduction-band nonparabolicity. As before, the tight-binding calculation assumes that the electrons are incident from the Γ valley of GaAs. Neither model faithfully reproduces the I-V characteristics of a RTD, for the current does not begin a strong monotonic increase after reaching a minimum. This is not, however, unexpected, since both models are coherent. In such models, the current will not rise again until the applied bias approaches the second resonance or becomes so great that the electron may tunnel over the barriers. Because much of the potential is dropped across the space-charge regions (as opposed to the RTD proper), in devices with small wells, the bias will necessarily be fairly high when the second resonance is reached. Since in both models the current is fairly flat after the first peak, it is reasonable to take an average for the valley current. In the tight-binding model, we have a peak current density of 3.10×10^5 A/cm^2 and an average valley current of 4948 A/cm^2, for a peak-to-valley ratio of about 63. In the envelope-function model, the peak current density is 1.57×10^5 A/cm^2 and the average valley current density is 434 A/cm^2, giving a peak-to-valley ratio of about 361. Note that these differences between the two models, as well as the tight-binding model's lower peak bias, are all explained by the tight-binding model's inclusion of the AlAs longitudinal X valleys. Since the X-valley barrier is quite low (about 0.077 eV with our parameters), its inclusion will tend to make the RTD more transparent.

IV. CONCLUSIONS

In order to model modern quantum devices more realistically, it is essential to treat heterointerfaces more carefully than is possible in the usual envelope-function approximation. It is also often necessary to take into account band nonparabolicity and the effects of multiple valleys and bands. Because the conduction-band discontinuity between the AlAs X valley and the GaAs Γ valley is rather small, inclusion of multivalley effects can become important for heterostructures, especially RTD's. A RTD model that takes into account the rather small barrier presented by the AlAs X valley will lead to a structure which is much more transparent to electron tunneling, resulting in larger valley currents. In order to include space-charge regions in our model, we have presented an improved method for carrying out transfer-matrix calculations which allows one to transfer across relatively large distances (> 1000 Å) and incorporate all of the important regions of the device. Our transmission coefficients calculated using the tight-binding model show extra structure associated with X valley tunneling which does not, however, significantly manifest itself in the

current-voltage characteristics. We have also found that while the tight-binding model predicts significantly higher valley currents than does the envelope-function model, leading to a more realistic peak-to-valley ratio, it still fails to satisfactorily reproduce the I-V characteristics of a RTD. Thus, while the tight-binding model clearly represents an improvement over the envelope-function model, a complete description of a RTD will need to include additional effects, such as self-consistently determined potentials, phonons, interface roughness, and impurity scattering.

ACKNOWLEDGMENTS

We would like to thank Professor Walter Harrison for his helpful suggestions and Byung Park, Robert Lodenkamper, and Ed Wolak for discussions. We would also like to thank Digital Equipment Corporation for helping fund the purchase of the computers on which many of these simulations were run. This work was supported by U.S. Office of Naval Research, U.S. Defense Advanced Research Projects Agency under Contract No. N00014-C-83-0077.

[1]T. Ando, S. Wakahara, and H. Akera, Phys. Rev. B **40**, 11 609 (1989).

[2]T. Ando and H. Akera, Phys. Rev. B **40**, 11 619 (1989).

[3]G. C. Osbourn and D. L. Smith, Phys. Rev. B **15**, 2124 (1979).

[4]J. N. Schulman and Yia-Chung Chang, Phys. Rev. B **31**, 2056 (1985).

[5]Kenneth V. Rousseau, K. L. Wang, and J. N. Schulman, Appl. Phys. Lett. **54**, 1341 (1989).

[6]D. H. Lee and J. D. Joannopoulos, Phys. Rev. B **23**, 4988 (1981).

[7]D. H. Lee and J. D. Joannopoulos, J. Vac. Sci. Technol. **19**, 355 (1981).

[8]J. N. Schulman and Yia-Chung Chang, Phys. Rev. B **27**, 2346 (1983).

[9]P. Vogl, H. P. Hjalmarson, and J. D. Dow, J. Phys. Chem. Solids **44**, 365 (1983).

[10]MAPLE was developed by the Symbolic Computation Group, Department of Computer Science, University of Waterloo, Waterloo, Ontario, Canada. We used Version 4.2 running on an Amiga 2500 microcomputer.

[11]N. W. Ashcroft and N. D. Mermin, *Solid State Physics* (Saunders, Philadelphia, 1976).

[12]We have modified a version of ACM Algorithm 533, by Andrew H. Sherman. See Andrew H. Sherman, ACM Trans. Math. Software **4**, 330 (1978); and Andrew H. Sherman, NSPIV, *A Fortran Subroutine for Sparse Gaussian Elimination With Partial Pivoting,* Vol. III of *Collected Algorithms from ACM* (Association for Computing Machinery, New York, 1983).

[13]R. Tsu and L. Esaki, Appl. Phys. Lett. **22**, 562 (1973).